







Ti-fraction-induced electronic and magnetic transformations in titanium oxide films

Cite as: J. Chem. Phys. **150**, 154704 (2019); <https://doi.org/10.1063/1.5089697>

Submitted: 22 January 2019 . Accepted: 28 March 2019 . Published Online: 16 April 2019

Meiling Xu , Xin Zhong, Jian Lv , Wenwen Cui, Jingming Shi , V. Kanchana , G. Vaitheeswaran, Jian Hao, Yanchao Wang , and Yinwei Li 



View Online



Export Citation



CrossMark

ARTICLES YOU MAY BE INTERESTED IN

[Energetics of counterion adsorption in the electrical double layer](#)

The Journal of Chemical Physics **150**, 154706 (2019); <https://doi.org/10.1063/1.5087835>

[Theoretical study of the absolute inner-shell photoionization cross sections of the formic acid and some of its hydrogen-bonded clusters](#)

The Journal of Chemical Physics **150**, 154308 (2019); <https://doi.org/10.1063/1.5088491>

[Van der Waals density functional study of formic acid adsorption and decomposition on Cu\(111\)](#)

The Journal of Chemical Physics **150**, 154707 (2019); <https://doi.org/10.1063/1.5087420>

The Journal
of Chemical Physics

2018 EDITORS' CHOICE

READ NOW!



Ti-fraction-induced electronic and magnetic transformations in titanium oxide films

Cite as: J. Chem. Phys. 150, 154704 (2019); doi: 10.1063/1.5089697

Submitted: 22 January 2019 • Accepted: 28 March 2019 •

Published Online: 16 April 2019



Meiling Xu,^{1,2} Xin Zhong,³ Jian Lv,^{4,a)} Wenwen Cui,¹ Jingming Shi,¹ V. Kanchana,⁵
G. Vaitheeswaran,^{6,7} Jian Hao,¹ Yanchao Wang,⁴ and Yinwei Li^{1,2,a)}

AFFILIATIONS

¹Laboratory of Quantum Materials Design and Application, School of Physics and Electronic Engineering, Jiangsu Normal University, Xuzhou 221116, China

²Jiangsu Key Laboratory of Advanced Laser Materials and Devices, Jiangsu Normal University, Xuzhou 221116, China

³Key Laboratory of Functional Materials Physics and Chemistry of the Ministry of Education, Jilin Normal University, Changchun 130103, China

⁴State Key Lab of Superhard Materials & Innovation Center of Computational Physics Methods and Software, College of Physics, Jilin University, Changchun 130012, China

⁵Department of Physics, Indian Institute of Technology Hyderabad, Kandi, Sangareddy 502285, Telangana, India

⁶School of Physics, University of Hyderabad, Prof. C. R. Rao Road, Gachibowli, Hyderabad 500046, Telangana, India

⁷Advanced Center for Research on High Energy Materials (ACRHEM), University of Hyderabad, Prof. C. R. Rao Road, Gachibowli, Hyderabad, Telangana 500046, India

^{a)}Authors to whom correspondence should be addressed: lvjian@calypso.cn and yinwei_li@jsnu.edu.cn

ABSTRACT

Titanium dioxide has been widely used in modern industrial applications, especially as an effective photocatalyst. Recently, freestanding TiO₂ films with a markedly reduced bandgap of ~1.8 eV have been synthesized, indicating that the dimension has a considerable influence on the bulk band gap (>~3 eV) and enhances the adsorption range of visible light. Titanium oxide compounds have various stoichiometries and versatile properties. Therefore, it is very necessary to explore the electronic properties and functionalities of other titanium oxide films with different stoichiometries. Here, we combined structure searches with first-principle calculations to explore candidate Ti–O films with different stoichiometries. In addition to the experimentally synthesized TiO₂ film, the structure searches identified three new energetically and dynamically stable Ti–O films with stoichiometries of Ti₃O₅, Ti₃O₂, and Ti₂O. Calculations show that the Ti–O films undergo several interesting electronic transformations as the Ti fraction increases, namely, from a wide-gap semiconductor (TiO₂, 3.2 eV) to a narrow-gap semiconductor (Ti₃O₅, 1.80 eV) and then to metals (Ti₃O₂ and Ti₂O) due to the abundance of unpaired Ti-*d* electrons. In addition to the electronic transformations, we observed nonmagnetic (TiO₂) to ferromagnetic (Ti₃O₅, Ti₃O₂, and Ti₂O) transformations. Notably, the Ti₃O₅ film possesses both narrow-gap semiconductive and ferromagnetic properties, with a large magnetic moment of 2.0 μ_B per unit cell; therefore, this film has high potential for use in applications such as spintronic devices. The results highlight metal fraction-induced electronic and magnetic transformations in transition metal oxide films and provide an alternative route for the design of new, functional thin-film materials.

Published under license by AIP Publishing. <https://doi.org/10.1063/1.5089697>

I. INTRODUCTION

Ultrathin two-dimensional (2D) nanomaterials have emerged as promising candidates for various applications, such as electronics/optoelectronics, electrocatalysts, photocatalysts, supercapacitors,

solar cells, and sensing platforms, due to their low-dimensional nature and unprecedented physicochemical properties.^{1–6} Dozens of 2D nanomaterials have been successfully synthesized or exfoliated by various well-developed synthetic methods, which can be divided into two strategies: top-bottom and bottom-up

methods.^{7–12} Notably, both types of methods are applicable only to layer-structured bulk materials and are useless for many nonlayered metal oxides.

Recently, Zavabeti *et al.* designed a liquid metal-based reaction route that can effectively isolate metal oxide thin films from bulk materials, such as HfO₂, Al₂O₃, and Gd₂O₃.¹³ Subsequently, Wang *et al.* reported the successful synthesis of a freestanding 2D titanium dioxide (TiO₂) film via a one-step solvothermal method.¹⁴ These experimental methods provided the framework for exploring free-standing 2D materials isolated from nonlayer-structured bulk metal oxides.

As a typical metal oxide, TiO₂ has attracted considerable research interest in the photovoltaic field due to its long-term stability, nontoxic environmental acceptability, and broad, low cost availability.^{15–21} However, TiO₂ is photoactive only in the range of the ultraviolet region because of its wide band gap of ~3 eV.^{22,23} Numerous research efforts have been devoted to narrowing the bandgap of TiO₂ to absorb light in a broader spectral range by doping or reduction.^{24–32} However, the dopants not only induce impurity states (donor or acceptor) in the midgap region but can also serve as charge carrier traps or recombination centers, which are detrimental to photocatalytic performance. Several studies have shown that TiO_{2-x} exhibits several intriguing properties and that Ti³⁺ can trigger the emergence of conduction, superconductivity, and magnetism.^{33–35} Thus, the question arises of whether a new strategy with high experimental feasibility can be developed to intrinsically adjust the electronic and even magnetic properties of titanium dioxides.

It is noted that stoichiometry has an important influence on structures and properties of materials.^{36–39} In this study, we systematically investigated freestanding Ti–O films with various stoichiometries using a global optimization swarm-intelligence algorithm combined with first-principle calculations. Notably, our structure searches revealed three new Ti-rich films with stoichiometries of Ti₃O₅, Ti₃O₂, and Ti₂O, which are confirmed to be energetically and dynamically stable. Electronic transitions from a wide-gap semiconductor (TiO₂, 3.2 eV) to a narrow-gap semiconductor (Ti₃O₅, 1.80 eV) and then to metals (Ti₃O₂ and Ti₂O) occur as the Ti fraction increases. Simultaneously, we observed a peculiar non-magnetic to ferromagnetic transition with the Ti fraction increasing from TiO₂ to Ti₃O₅, Ti₃O₂, and Ti₂O. As a result, the Ti₃O₅ film becomes a ferromagnetic narrow-gap semiconductor with a large magnetic moment of 2.0 μ_B per unit cell, thereby displaying great potential for use in novel spintronic devices such as infrared detectors.

II. COMPUTATIONAL METHODS

The search for various 2D phases of Ti–O films (Ti = 1–4 and O = 1–5) has largely relied on swarm-intelligence-based CALYPSO (Crystal structure AnaLYsis by Particle Swarm Optimization) software,^{40,41} which is designed to search for the stable structures of given compounds.^{42–49} The underlying structural relaxations and electronic structure calculations are performed using the spin-polarized plane-wave pseudopotential method, as implemented in the Vienna *ab initio* simulation package (VASP).⁵⁰ The Perdew-Burke-Ernzerhof (PBE) generalized gradient approximation⁵¹ is chosen for the exchange-correlation functional, and a Hubbard U

term ($U = 4.5$ eV)⁵² is considered to address the self-interaction error of the generalized gradient approximation. The electron-ion interactions are described by projector augmented-wave pseudopotentials,⁵³ with $3p^6 3d^3 4s^1$ and $2s^2 2p^4$ configurations treated as the valence electrons for Ti and O, respectively. A kinetic cutoff energy of 500 eV and Monkhorst-Pack k meshes with a grid spacing of $2\pi \times 0.03 \text{ \AA}^{-1}$ are adopted to obtain converged total energies (~1 meV/atom). In the electronic structure computation, the GGA + U ($U = 4.5$ eV)⁵² method is used to accurately obtain the energy band gap. The dynamic stability of the predicted new phases was verified from phonon calculations using the direct supercell method, as implemented in the PHONOPY code.^{54,55} To check the thermal stability, *ab initio* molecular dynamic (AIMD) simulations were carried out with a time step of 1 fs and total simulation time of 6 ps. The temperature was controlled at 300 K using the Nosé-Hoover chain thermostat.

III. RESULTS AND DISCUSSION

A. Energetic stability of Ti–O films

The relative stabilities of the various 2D phases of Ti–O films are determined according to their calculated formation enthalpy, which is defined as

$$E_{\text{formation}} = \frac{1}{N} (E_{\text{tot}} - \sum n_i \mu_i), \quad (1)$$

where E_{tot} is the total energy of a candidate structure, n_i is the number of atoms, μ_i is the chemical potential for each atomic species, and N is the number of atoms per formula unit and serves as a normalization factor.

The chemical potentials (μ_{O} and μ_{Ti}) must satisfy the following boundary constraints:

$$(i) \mu_{\text{Ti}} \leq \mu_{\text{Ti}}^{\text{bulk}},$$

$$(ii) \mu_{\text{O}} \leq \frac{1}{2} \mu_{\text{O}_2},$$

$$(iii) \mu_{\text{Ti}} + 2\mu_{\text{O}} = E_{\text{TiO}_2},$$

where E_{TiO_2} is the internal energy of the bulk rutile phase. Equation (1) can thus be written as follows:

$$E_{\text{formation}} = \frac{1}{N} [E_{\text{tot}} - n_{\text{Ti}} E_{\text{TiO}_2} - \mu_{\text{O}} (n_{\text{O}} - 2n_{\text{Ti}})]. \quad (2)$$

According to the constraints of the chemical potential, the range of μ_{O} is set as follows:

$$\frac{1}{2} \mu_{\text{O}_2} \geq \mu_{\text{O}} \geq \frac{1}{2} (E_{\text{TiO}_2} - \mu_{\text{Ti}}). \quad (3)$$

Thus, the most stable 2D phase of Ti–O films for different chemical potentials of oxygen can be identified.

The experimentally synthesized lepidocrocite structure of the TiO₂ film¹⁴ is readily predicted in the proposed structure searches, confirming the validity of the search method. The dependence of the total energy on the chemical potential of oxygen is shown in Fig. 1. Stable structures are those possessing the lowest formation enthalpy at a certain range of chemical potentials. In addition to TiO₂ ($-4.15 \text{ eV} \leq \Delta\mu_{\text{O}} < 0 \text{ eV}$), three new stable 2D Ti–O films with

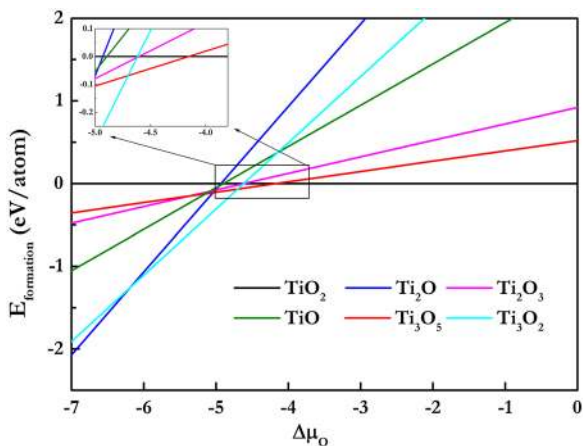


FIG. 1. Calculated formation energies of various film structures as a function of the chemical potential of oxygen with respect to the TiO_2 film.

high Ti fractions exist: Ti_3O_5 ($-4.70 \text{ eV} \leq \Delta\mu_{\text{O}} < -4.15 \text{ eV}$), Ti_3O_2 ($-6.19 \text{ eV} \leq \Delta\mu_{\text{O}} < -4.70 \text{ eV}$), and Ti_2O ($\Delta\mu_{\text{O}} < -6.19 \text{ eV}$).

The μ_{O} value at a given pressure and temperature can be defined as $\mu_{\text{O}} = \frac{1}{2}[E_{\text{O}_2} + \Delta H_{\text{O}_2}(T, P^0) - T\Delta S_{\text{O}_2}(T, P^0) + k_{\text{B}}T \ln(P/P^0)]$, where k_{B} , P^0 , and P are the Boltzmann constant, standard atmospheric pressure, and oxygen partial pressure, respectively. $\Delta H_{\text{O}_2}(T, P^0)$ and $T\Delta S_{\text{O}_2}(T, P^0)$ are taken from the NIST chemistry database.⁵⁶ According to the above equation, to synthesize Ti-richer Ti–O films with $\Delta\mu_{\text{O}}$ values less than -7 eV , a temperature of 5000 K and an ultrahigh vacuum level of $\sim 10^{-18} \text{ p}^0$ are needed, which are experimentally impossible to achieve. Therefore, Ti–O films with high Ti fractions are not considered in our calculations.

B. Geometric structures of Ti–O films

The predicted stable structures and structural parameters are shown in Fig. 2 and Table S1, respectively. Specifically, the TiO_2 film is a monolayer isolated from the lepidocrocite structure of TiO_2 and consists of TiO_6 octahedrons with all Ti atoms in six-fold ($\text{Ti}_{6\text{c}}$) coordination. With increasing Ti fraction, the number of dangling

bonds of Ti atoms increases, leading to six ($\text{Ti}_{6\text{c}}$)-, five ($\text{Ti}_{5\text{c}}$)-, and four-fold ($\text{Ti}_{4\text{c}}$) coordinations of Ti atoms [Fig. 2(b)]. The similar coordinations of Ti atoms in the TiO_2 and Ti_3O_5 films result in similar thicknesses and average Ti–O bond lengths, e.g., thicknesses of 4.33 \AA and 4.35 \AA and bond lengths of 2.02 \AA and 2.04 \AA for the TiO_2 and Ti_3O_5 films, respectively (Table I). The Ti_3O_2 film is composed of two TiO layers intercalated by a Ti layer, and the coordination numbers of Ti atoms decrease by four ($\text{Ti}_{4\text{c}}$)- and two-fold ($\text{Ti}_{2\text{c}}$) due to the further increase in the Ti fraction [Fig. 2(c)]. Ti_2O is constructed with a TiO layer and a Ti layer, in which Ti atoms are in two ($\text{Ti}_{2\text{c}}$)- and one-fold ($\text{Ti}_{1\text{c}}$) coordinations, respectively. Notably, we found that the structure of Ti_2O can be obtained by removing one TiO layer in the Ti_3O_2 film. This result is expected if we consider that Ti_2O can be derived by removing TiO from Ti_3O_2 . As a result, the thickness of Ti_2O (2.60 \AA) is nearly half that (5.66 \AA) of the Ti_3O_2 film. The lower coordination states of Ti atoms in Ti-rich Ti_3O_2 and Ti_2O films lead to longer Ti–O lengths, e.g., 2.46 \AA and 2.35 \AA for Ti_3O_2 and Ti_2O , respectively. It is found that the average Ti–O bond length of the TiO_2 film is close to those of bulk phases, while Ti_3O_5 , Ti_3O_2 , and Ti_2O films possess longer Ti–O bonds. With the Ti fraction increasing, we found that the coordination number of Ti atom becomes more complex, with the formation of $\text{Ti}_{5\text{c}}$, $\text{Ti}_{4\text{c}}$, $\text{Ti}_{2\text{c}}$, and $\text{Ti}_{1\text{c}}$ (Table S2).

C. Dynamical and thermal stability of Ti–O films

The calculated phonon dispersion curves and total phonon density of states (PHDOS) along the principal symmetry directions in the Brillouin zone are plotted in Fig. 3. There are no imaginary frequencies in the Brillouin zone, indicating that the Ti_3O_2 and Ti_2O films are dynamically stable. We note that the phonon band in the Ti_3O_5 film has small imaginary frequencies in the vicinity of the gamma point, as have been observed in other 2D materials,⁵⁷ such as SiGe and GaN. Such modes are of an acoustic nature and are derived from a collective vibration mode with a long wavelength approaching infinity; this mode has a negligible effect on the overall structural stability.^{57,58} For Ti_3O_2 and Ti_2O films, the main contributions to acoustic phonons and optical phonons result from the Ti cations and O anions, respectively. By contrast, the main contribution to acoustic phonons in the Ti_3O_5 film results from both Ti and O atoms, indicating strong Ti–O hybridization. The strong Ti–O hybridization

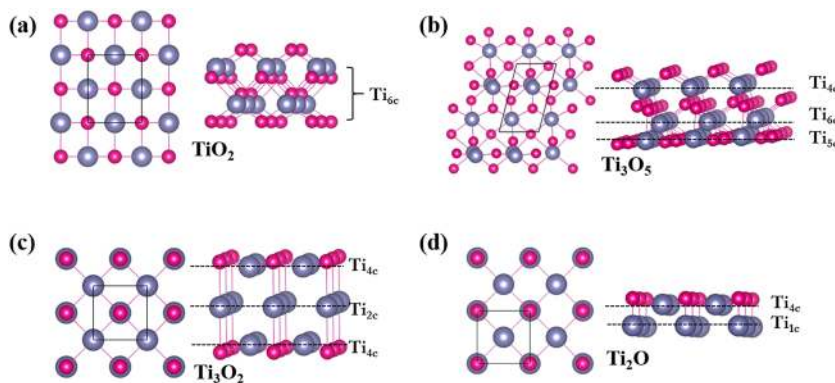
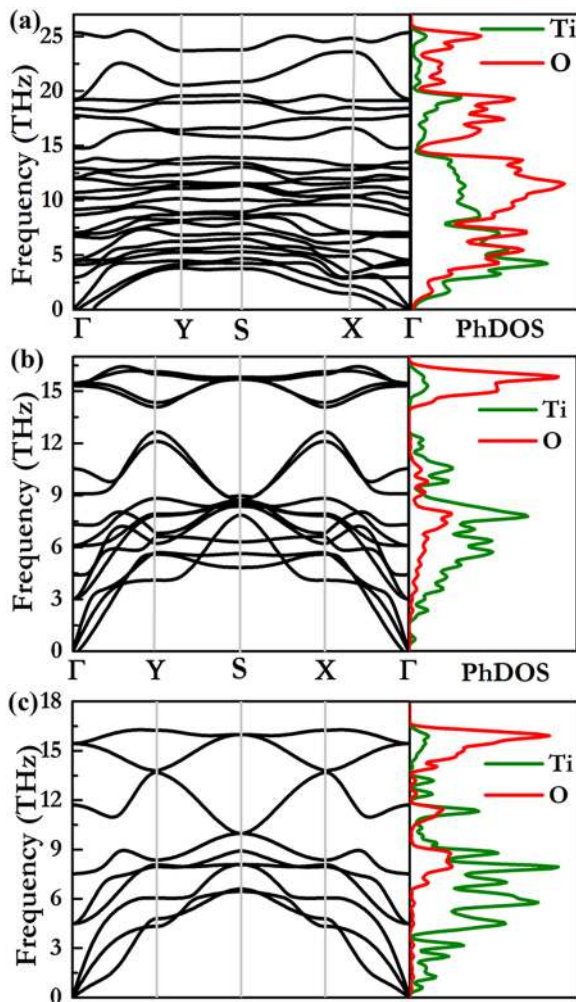


FIG. 2. Structures of the (a) TiO_2 , (b) Ti_3O_5 , (c) Ti_3O_2 , and (d) Ti_2O films. The atoms in dark gray and pink colors represent Ti and O atoms, respectively. As an example, the label “ $\text{Ti}_{6\text{c}}$ ” indicates that Ti atoms are characterized by six-fold coordination.

TABLE I. The stable range of the chemical potential (x), the thickness (t), the average bond length ($d_{\text{Ti-O}}$) of Ti-O bonds, and the Ti fraction (θ) in various Ti-O films.

	x (eV)	t (Å)	$d_{\text{Ti-O}}$ (Å)	θ (%)
TiO ₂	$-4.15 \leq x \leq 0$	4.33	2.02	33.3
Ti ₃ O ₅	$-4.70 \leq x < -4.15$	4.35	2.04	37.5
Ti ₃ O ₂	$-6.19 \leq x < -4.70$	5.66	2.46	60.0
Ti ₂ O	$x < -6.19$	2.60	2.35	66.7

is also reflected by the relatively short Ti-O bond lengths. Generally, polar surfaces are unstable because of the existence of a nonzero dipole moment perpendicular to the surface, which leads to reconstruction or defect. In fact, experiments have also observed

**FIG. 3.** The phonon dispersions and PHDOS values of the (a) Ti₃O₅, (b) Ti₃O₂, and (c) Ti₂O films. High-symmetry q-point paths: $\Gamma(0, 0) \rightarrow Y(-1/2, 0) \rightarrow S(-1/2, 1/2) \rightarrow X(0, 1/2) \rightarrow \Gamma(0, 0)$.

several polar ZnO surfaces that are stable without reconstruction.⁵⁹ Here, we have performed AIMD simulations to check the thermal stability of the Ti₂O film at 300 K. No structure reconstructions are found after 6 ps with a time step of 1 fs, indicating the thermal stability of the Ti₂O film (Fig. S1).

D. Electronic and magnetic properties of Ti-O films

To provide detailed insight into the electronic properties of the stable 2D phases of Ti-O films, we calculated the spin-polarized band structures and projected density of states (PDOS), as shown in Fig. 4. Since the PBE functional typically underestimates the energy band gap, the PBE + U method with $U = 4.5$ eV is used to obtain accurate electronic structures.

1. Semiconductor to metal transition

We explored the electronic band structures and PDOS for all the Ti-O films and observed interesting electronic transformations as the Ti fraction increases. As shown in Fig. 4(a), the TiO₂ film is a wide-gap semiconductor with a gap of 3.2 eV, which is smaller than that (3.52 eV) of bulk lepidocrocite phase (Table S2). In contrast to TiO₂, two flat surface bands form below the Fermi level in the Ti₃O₅ film [Fig. 4(b)] and are occupied by unpaired Ti d electrons. This result is expected since the increased Ti fraction reduces the coordination numbers of Ti atoms in the top and bottom layers [Fig. 2(b)], which results in redundant electrons from Ti atoms. As a consequence, the band gap of the Ti₃O₅ film decreases to ~ 2 eV. As the Ti fraction further increases, the occurrence of more unpaired Ti d electrons contributes to the formation of more surface bands. As expected, the Ti₃O₂ and Ti₂O films display metallic properties, with several bands crossing the Fermi levels [Figs. 4(c) and 4(d)].

2. Nonmagnetic to ferromagnetic transition

The valence electron configurations considered for Ti and O atoms are $3p^6 3d^3 4s^1$ and $2s^2 2p^4$, respectively. For the TiO₂ film, Ti is a quadrivalent cation with a d^0 electron count. The empty d orbitals of the Ti cation lead to a nonmagnetic structure as reflected by the calculated spin-up and spin-down DOSs [Fig. 4(a)], which is consistent with bulk phases (Table S2). Fig. 4(b) clearly shows that the Ti₃O₅ film is a ferromagnetic semiconductor with two surface bands occupied by spin-up electrons. In Ti₃O₅, two unpaired d electrons left for Ti cations alternatively occupy the two surface bands, which reasonably leads to the high-spin state of Ti atoms, with a magnetic moment of $2 \mu_B$ per unit cell. As expected, the calculated total magnetic moment of the Ti atoms is $1.98 \mu_B$ per unit cell. Simultaneously, we observed a slight spin polarization of O $2p$ electrons with a uniform moment of $0.02 \mu_B$ per unit cell, which originates from the hybridization between Ti $3d$ and O $2p$ orbitals.

As shown in Fig. 4(c), the Ti₃O₂ film is slightly magnetic, and the calculated magnetic moment is approximately $0.08 \mu_B$ per unit cell. Spin polarization and the overlap between spin-up and spin-down states around the Fermi level are also observed in the PDOS of the Ti₂O film [Fig. 4(d)]. The calculated total magnetic moment of the Ti atoms is $0.5 \mu_B$ per unit cell. Two nonequivalent Ti atoms in the Ti₂O compound result in different magnetic moments: $1.0 \mu_B$ for Ti_{4c} and $-0.5 \mu_B$ for Ti_{1c} in a unit cell.

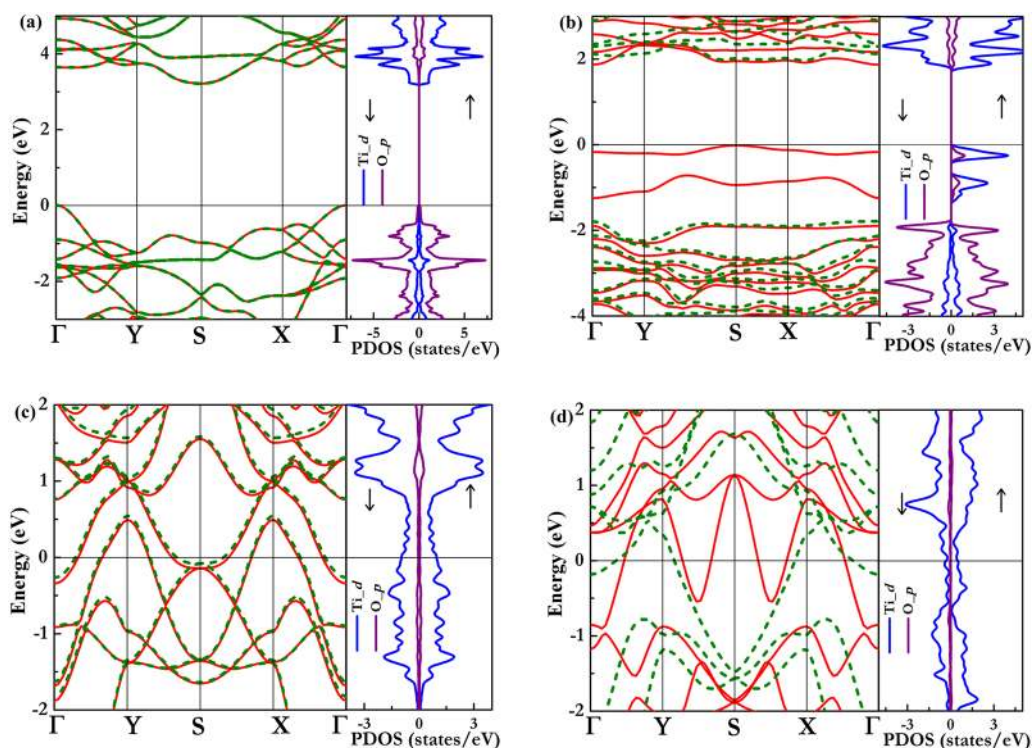


FIG. 4. Spin-polarized band structures and PDOS for the (a) TiO_2 , (b) Ti_3O_5 , (c) Ti_3O_2 , and (d) Ti_2O films. The red lines and green dashed lines represent spin-up and spin-down components, respectively. The zero energy indicates the Fermi level or the top valence band for metallic or semiconducting structures, respectively. \uparrow and \downarrow represent spin-up and spin-down states, respectively.

3. The SOC effect on the electronic properties of Ti-O films

We also examined the spin-orbit coupling (SOC) effect on the electronic properties of Ti_3O_5 , Ti_3O_2 , and Ti_2O films with the

inclusion of Hubbard U . The inclusion of SOC slightly revised the band structures of the Ti_3O_5 and Ti_2O films (Fig. S2), reflecting the minor effect of SOC on the electronic properties of these two films. By contrast, SOC had a significant effect on the metallic Ti_3O_2

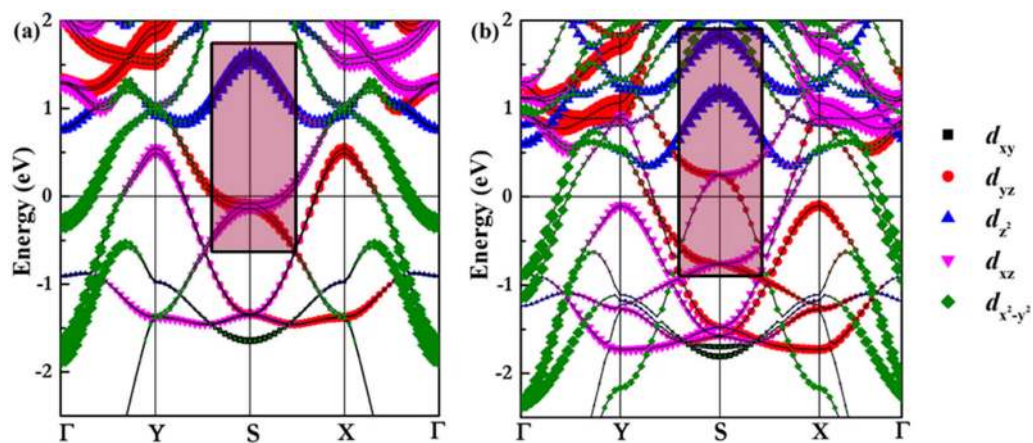


FIG. 5. Projected band structures of the Ti_3O_2 film without (a) and with (b) the inclusion of the SOC effect. The symbols indicate the contributions of split- d orbitals are proportional to the number of electrons. Shadow rectangles illustrate the splitting of d_{z^2} and d_{yz} , d_{xz} orbitals.

film, as demonstrated by the obvious change in the band profiles near the Fermi level (Fig. 5). The band structures of the Ti_3O_2 film have been projected on different Ti d (d_{xy} , d_{xz} , d_{z^2} , d_{yz} and d_{zx}) orbitals represented by different symbols and colors. The sizes of the symbols are proportional to the number of electrons. From Fig. 5(a), we can find two degenerate bands located at ~ 1.5 eV and 0.1 eV at the S point, which originated mainly from d_{z^2} and $d_{yz} + d_{xz}$ orbitals deduced from their large symbol sizes. As illustrated by the rectangles, the degenerate d_{z^2} and $d_{yz} + d_{xz}$ orbitals split when including SOC, with a splitting width of ~ 0.64 eV and 1 eV, respectively [Fig. 5(b) and Fig. S3]. The spin-degenerate parabolic bands split into dispersions with oppositely spin-polarized states due to the SOC effect, which evokes the Rashba effect.⁶⁰ Generally, this effect has been demonstrated in semiconductor heterostructures,⁶¹ two-dimensional electron gases,⁶⁰ and heavy element-based surface alloys.⁶²

IV. CONCLUSIONS

In summary, we systemically explored candidate freestanding 2D Ti–O films in Ti-rich conditions compared to known TiO_2 using the swarm-intelligence-based CALYPSO method and first-principle calculations. Three new Ti–O films with stoichiometries of Ti_3O_5 , Ti_3O_2 , and Ti_2O were predicted to be stable under different conditions of the chemical potential of oxygen. Band structure calculations revealed that TiO_2 and Ti_3O_5 are semiconductors with band gaps of 3.2 eV and 1.80 eV, respectively. Notably, as the Ti fraction increases, Ti_3O_2 and Ti_2O display a metallic nature due to the increase in the redundant electrons of Ti atoms. Moreover, magnetic transformations in Ti–O films from nonmagnetic (TiO_2) to ferromagnetic (Ti_3O_5 , Ti_3O_2 , and Ti_2O) are found with increasing Ti fraction. Thus, the Ti_3O_5 film displays both narrow-gap semiconducting and ferromagnetic properties with a large magnetic moment of $2.0 \mu_B$ per unit cell and has great potential for applications involving spintronic devices. Our study provides an example of element fraction-induced electronic and magnetic transformations in nonlayer-structured metal oxide films and an alternative route for the design of new, functional thin-film materials.

SUPPLEMENTARY MATERIAL

See [supplementary material](#) for optimized structural parameters of Ti–O compounds; structural parameters and properties of bulk TiO_2 phases and Ti–O films; the AIMD simulations of Ti_2O film; band structures of Ti_3O_5 and Ti_2O films with and without the SOC effect; and the projected DOS of the Ti_3O_2 film.

ACKNOWLEDGMENTS

Y.L., M.X., and J.H. acknowledge funding from the National Natural Science Foundation of China under Grant Nos. 11722433 and 11404148 and the Qing Lan Project and Six Talent Peaks Project of Jiangsu Province. Y.W. and X.Z. acknowledge funding from the National Natural Science Foundation of China under Grant Nos. 11774127, 11822404, and 11704151; W.C. and J.S. acknowledge funding from the National Natural Science Foundation of China under Grant Nos. 11804128 and 11804129. Some of the calculations

were performed at the High-performance Computing Center of Jilin University and the School of Physics and Electronic Engineering of Jiangsu Normal University.

The authors declare no competing financial interests.

REFERENCES

- 1 C. Tan, X. Cao, X.-J. Wu, Q. He, J. Yang, X. Zhang, J. Chen, W. Zhao, S. Han, G.-H. Nam, M. Sindoro, and H. Zhang, *Chem. Rev.* **117**, 6225 (2017).
- 2 S. Manzeli, D. Ovchinnikov, D. Pasquier, O. V. Yazyev, and A. Kis, *Nat. Rev. Mater.* **2**, 17033 (2017).
- 3 M. Xu, Y. Chen, F. Xiong, J. Wang, Y. Liu, J. Lv, Y. Li, Y. Wang, Z. Chen, and Y. Ma, *J. Mater. Chem. A* **6**, 16087 (2018).
- 4 A. V. Rozhkov, A. L. Rakhmanov, A. O. Sboychakov, K. I. Kugel, and F. Nori, *Phys. Rev. Lett.* **119**, 107601 (2017).
- 5 L.-M. Yang, E. Ganz, Z. Chen, Z.-X. Wang, and P. V. R. Schleyer, *Angew. Chem., Int. Ed.* **54**, 9468 (2015).
- 6 L.-M. Yang, V. Bačić, I. A. Popov, A. I. Boldyrev, T. Heine, T. Frauenheim, and E. Ganz, *J. Am. Chem. Soc.* **137**, 2757 (2015).
- 7 M. Yi and Z. Shen, *J. Mater. Chem. A* **3**, 11700 (2015).
- 8 X. Li, W. Cai, J. An, S. Kim, J. Nah, D. Yang, R. Piner, A. Velamakanni, I. Jung, E. Tutuc, S. K. Banerjee, L. Colombo, and R. S. Ruoff, *Science* **324**, 1312 (2009).
- 9 V. Nicolosi, M. Chhowalla, M. G. Kanatzidis, M. S. Strano, and J. N. Coleman, *Science* **340**, 1226419 (2013).
- 10 W. S. Hummers and R. E. Offeman, *J. Am. Chem. Soc.* **80**, 1339 (1958).
- 11 J. H. Han, S. Lee, and J. Cheon, *Chem. Soc. Rev.* **42**, 2581 (2013).
- 12 M. Naguib, M. Kurtoglu, V. Presser, J. Lu, J. Niu, M. Heon, L. Hultman, Y. Gogotsi, and M. W. Barsoum, *Adv. Mater.* **23**, 4248 (2011).
- 13 A. Zavabeti, J. Z. Ou, B. J. Carey, N. Syed, R. Orrell-Trigg, E. L. H. Mayes, C. Xu, O. Kavehei, A. P. O'Mullane, R. B. Kaner, K. Kalantar-Zadeh, and T. Daeneke, *Science* **358**, 332 (2017).
- 14 S. L. Wang, X. Luo, X. Zhou, Y. Zhu, X. Chi, W. Chen, K. Wu, Z. Liu, S. Y. Quek, and G. Q. Xu, *J. Am. Chem. Soc.* **139**, 15414 (2017).
- 15 U. Diebold, *Surf. Sci. Rep.* **48**, 53 (2003).
- 16 B. O'Regan and M. Grätzel, *Nature* **353**, 737 (1991).
- 17 A. J. Bard and M. A. Fox, *Acc. Chem. Res.* **28**, 141 (1995).
- 18 L. Liu, H. Zhao, J. M. Andino, and Y. Li, *ACS Catal.* **2**, 1817 (2012).
- 19 H. Yaghoubi, N. Taghavinia, E. K. Alamdari, and A. A. Volinsky, *ACS Appl. Mater. Interfaces* **2**, 2629 (2010).
- 20 A. a. Ismail and D. W. Bahnemann, *J. Mater. Chem.* **21**, 11686 (2011).
- 21 A. Fujishima, X. Zhang, and D. A. Tryk, *Surf. Sci. Rep.* **63**, 515 (2008).
- 22 J. Pascual, J. Camassel, and H. Mathieu, *Phys. Rev. B* **18**, 5606 (1978).
- 23 A. Amtout and R. Leonelli, *Phys. Rev. B* **51**, 6842 (1995).
- 24 M. Anpo, *J. Catal.* **216**, 505 (2003).
- 25 X. Chen, S. Shen, L. Guo, and S. S. Mao, *Chem. Rev.* **110**, 6503 (2010).
- 26 S. G. Kumar and L. G. Devi, *J. Phys. Chem. A* **115**, 13211 (2011).
- 27 W. Choi, A. Termin, and M. R. Hoffmann, *J. Phys. Chem.* **98**, 13669 (1994).
- 28 Y. T. R. Asahi, T. Morikawa, T. Ohwaki, and K. Aoki, *Science* **293**, 269 (2001).
- 29 G. Wu, J. Wang, D. F. Thomas, and A. Chen, *Langmuir* **24**, 3503 (2008).
- 30 I. S. Cho, C. H. Lee, Y. Feng, M. Logar, P. M. Rao, L. Cai, D. R. Kim, R. Sinclair, and X. Zheng, *Nat. Commun.* **4**, 1723 (2013).
- 31 Y. Gai, J. Li, S. S. Li, J. B. Xia, and S. H. Wei, *Phys. Rev. Lett.* **102**, 036402 (2009).
- 32 J. Zhang, C. Pan, P. Fang, J. Wei, and R. Xiong, *ACS Appl. Mater. Interfaces* **2**, 1173 (2010).
- 33 H. W. Jang, D. A. Felker, C. W. Bark, Y. Wang, M. K. Niranjan, C. T. Nelson, Y. Zhang, D. Su, C. M. Folkman, S. H. Baek, S. Lee, K. Janicka, Y. Zhu, X. Q. Pan, D. D. Fong, E. Y. Tsybmal, M. S. Rzechowski, and C. B. Eom, *Science* **331**, 886 (2011).
- 34 Y. Li, Y. Weng, X. Yin, X. Yu, S. R. S. Kumar, N. Wehbe, H. Wu, H. N. Alshareef, S. J. Pennycook, M. B. H. Breese, J. Chen, S. Dong, and T. Wu, *Adv. Funct. Mater.* **28**, 1705657 (2018).

- ³⁵N. Reyren, S. Thiel, A. D. Caviglia, L. Fitting Kourkoutis, G. Hammerl, C. Richter, C. W. Schneider, T. Kopp, A. S. Rüetschi, D. Jaccard, M. Gabay, D. A. Muller, J. M. Triscone, and J. Mannhart, *Science* **317**, 1196 (2007).
- ³⁶K. Hameeuw, G. Cantele, D. Ninno, F. Trani, and G. Iadonisi, *Phys. Status Solidi* **203**, 2219 (2006).
- ³⁷W. J. Kim, M. H. Han, S. Lebègue, E. K. Lee, and H. Kim, *Front. Chem.* **7**, 47 (2019).
- ³⁸L. Chiodo, J. M. García-Lastra, A. Iacomino, S. Ossicini, J. Zhao, H. Petek, and A. Rubio, *Phys. Rev. B* **82**, 045207 (2010).
- ³⁹X. Zhao, S. Selcuk, and A. Selloni, *Phys. Rev. Mater.* **2**, 015801 (2018).
- ⁴⁰Y. Wang, M. Miao, J. Lv, L. Zhu, K. Yin, H. Liu, and Y. Ma, *J. Chem. Phys.* **137**, 224108 (2012).
- ⁴¹Y. Wang, J. Lv, L. Zhu, S. Lu, K. Yin, Q. Li, H. Wang, L. Zhang, and Y. Ma, *J. Phys. Condens. Matter* **27**, 203203 (2015).
- ⁴²J. Lv, Y. Wang, L. Zhu, and Y. Ma, *Phys. Rev. Lett.* **106**, 051503 (2011).
- ⁴³L. Zhu, H. Wang, Y. Wang, J. Lv, Y. Ma, Q. Cui, Y. Ma, and G. Zou, *Phys. Rev. Lett.* **106**, 145501 (2011).
- ⁴⁴Y. Li, X. Feng, H. Liu, J. Hao, S. A. T. Redfern, W. Lei, D. Liu, and Y. Ma, *Nat. Commun.* **9**, 722 (2018).
- ⁴⁵L. Zhu, H. Liu, C. J. Pickard, G. Zou, and Y. Ma, *Nat. Chem.* **6**, 644 (2014).
- ⁴⁶H. Wang, J. S. Tse, K. Tanaka, T. Iitaka, and Y. Ma, *Proc. Natl. Acad. Sci. U. S. A.* **109**, 6463 (2012).
- ⁴⁷Y. Li, J. Hao, H. Liu, J. S. Tse, Y. Wang, and Y. Ma, *Sci. Rep.* **5**, 9948 (2015).
- ⁴⁸Y. Li, J. Hao, H. Liu, Y. Li, and Y. Ma, *J. Chem. Phys.* **140**, 174712 (2014).
- ⁴⁹J. Lv, M. Xu, S. Lin, X. Shao, X. Zhang, Y. Liu, Y. Wang, Z. Chen, and Y. Ma, *Nano Energy* **51**, 489 (2018).
- ⁵⁰G. Kresse and J. Furthmüller, *Phys. Rev. B* **54**, 11169 (1996).
- ⁵¹J. P. Perdew, K. Burke, and M. Ernzerhof, *Phys. Rev. Lett.* **77**, 3865 (1996).
- ⁵²S. L. Dudarev, G. Botton, S. Y. Savrasov, C. J. Humphreys, and A. P. Sutton, *Phys. Rev. B* **57**, 1505 (1998).
- ⁵³G. Kresse and D. Joubert, *Phys. Rev. B* **59**, 1758 (1999).
- ⁵⁴K. Parlinski, Z. Li, and Y. Kawazoe, *Phys. Rev. Lett.* **78**, 4063 (1997).
- ⁵⁵A. Togo, F. Oba, and I. Tanaka, *Phys. Rev. B* **78**, 134106 (2008).
- ⁵⁶See <http://webbook.nist.gov/> for NIST Webbook.
- ⁵⁷H. Şahin, S. Cahangirov, M. Topsakal, E. Bekaroglu, E. Akturk, R. T. Senger, and S. Ciraci, *Phys. Rev. B* **80**, 155453 (2009).
- ⁵⁸S. Cahangirov, M. Topsakal, E. Aktürk, H. Şahin, and S. Ciraci, *Phys. Rev. Lett.* **102**, 236804 (2009).
- ⁵⁹O. Dulub, L. A. Boatner, and U. Diebold, *Surf. Sci.* **519**, 201 (2002).
- ⁶⁰K. Ishizaka, M. S. Bahramy, H. Murakawa, M. Sakano, T. Shimojima, T. Sonobe, K. Koizumi, S. Shin, H. Miyahara, A. Kimura, K. Miyamoto, T. Okuda, H. Namatame, M. Taniguchi, R. Arita, N. Nagaosa, K. Kobayashi, Y. Murakami, R. Kumai, Y. Kaneko, Y. Onose, and Y. Tokura, *Nat. Mater.* **10**, 521 (2011).
- ⁶¹J. Nitta, T. Akazaki, H. Takayanagi, and T. Enoki, *Phys. Rev. Lett.* **78**, 1335 (1997).
- ⁶²C. R. Ast, J. Henk, A. Ernst, L. Moreschini, M. C. Falub, D. Pacilé, P. Bruno, K. Kern, and M. Gironi, *Phys. Rev. Lett.* **98**, 186807 (2007).